Velocity and Angular Distributions of Prompt Neutrons from Spontaneous Fission of Cf^{252}

HARRY R. BOWMAN, STANLEY G. THOMPSON, J. C. D. MILTON, AND WLADYSLAW J. SWIATECKI
Lawrence Radiation Laboratory, University of California, Berkeley, California

(Received January 15, 1962)

The velocity and angular distributions of neutrons associated with light and heavy groups of fission fragments from spontaneous fission of Cf^{252} have been measured. The results can be accounted for within about 10 to 20% by the assumption of isotropic evaporation from moving fragments. Least-squares fits to the data have been made on this assumption and yield accurate values for the numbers of neutrons emitted by the light and heavy fragments and for their energy spectra. The energy spectra have been analyzed in terms of effective temperatures of the fragments. A detailed discussion of the systematic differences from simple evaporation theory is given.

I. INTRODUCTION

THE purpose of these experiments was to study the details of prompt neutron emission in the spontaneous fission of Cf^{252}. The approach used involved coincident measurements of neutron and fission-fragment flight times over a known distance. Measurement of the velocities of both fragments determines their masses and energies. Simultaneous measurement of the velocities of coincident neutrons making known angles with the fragment direction gives the basic information bearing on neutron emission in the fission process. Comparison of such measurements made at several angles might make it possible to distinguish between neutrons evaporated from the fully accelerated fragments and those emitted very much earlier in the fission process. It should also be possible to make a rather accurate determination of the energy spectrum of the evaporated neutrons in a frame of reference moving with the fragment.

In this paper the fragments are separated into only two groups, light and heavy; the correlations with fragment energy and mass division are the subject of another paper.

II. EXPERIMENTAL PROCEDURE

The velocities of fragments and neutrons were determined by measuring their flight times over a known distance. These flight times, ranging from about 20 to 200 nsec, were attained through the use of time-to-pulse-height converters of conventional design,[1] in which time is measured by the amount of charge collected on a condenser in the interval between two timing pulses. In this case the time-zero pulse (or time of fission) was formed from the secondary electrons emitted[2,3] when one of the fragments passed through a thin nickel foil placed as close as possible to the source. These electrons were focused and accelerated to 10 kev by an electron lens[3] and were finally detected by a thin plastic scintillator, 5 mils thick. Both the fragments and the neutrons were detected at the ends of their paths by plastic scintillators.

A. General Description of Apparatus

A schematic drawing of the apparatus is given in Fig. 1. The end-of-flight detectors were all mounted on the circumference of a 100-cm radius steel drum evacuated to a pressure of approx 10^{-6} mm Hg. There were four such detectors. Two neutron detectors, N_1, N_2 (pilot B plastic scintillators, 4 in. in diam, 2 in. thick) and two fission-fragment detectors F_1, F_2 (plastic scintillators, 4 in. in diam, 5 mils thick) were operated simultaneously. Time-of-flight measurements were made

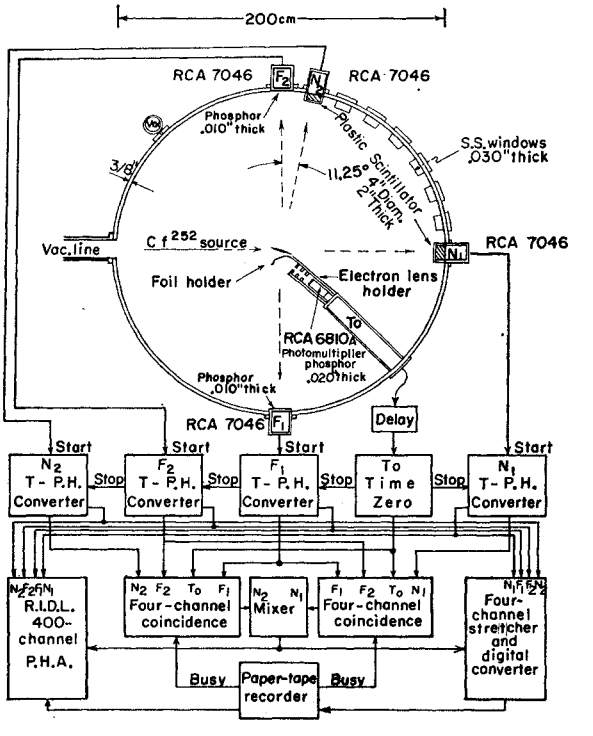

FIG. 1. Block diagram of the apparatus used to measure the velocities and angular distribution of prompt neutrons relative to fission fragments.

[1] W. Weber, C. W. Johnstone, and L. Cranberg, Rev. Sci. Instr. 27, 166 (1956).
[2] W. E. Stein and R. B. Leachman, Rev. Sci. Instr. 27, 1049 (1956).
[3] J. S. Fraser and J. C. D. Milton, Nuclear Instr. 2, 275 (1958).

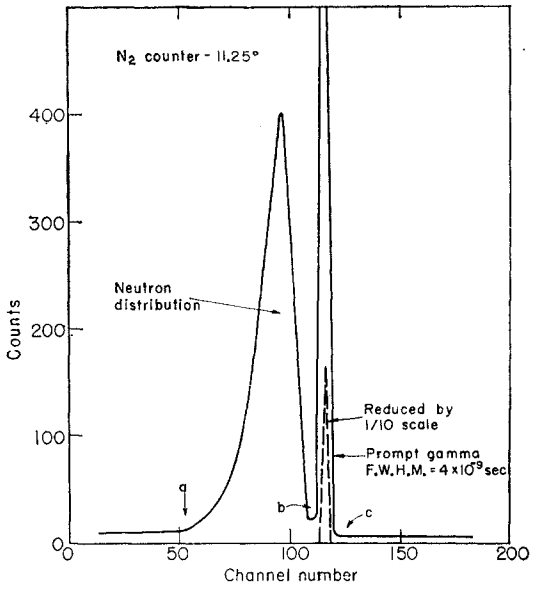

FIG. 2. Time-of-flight distribution of neutrons and γ rays measured at 11.25 deg in coincidence with fission fragments.

for those events in which one neutron and two fragments occurred in coincidence. Rare events in which two neutrons were detected in coincidence with both fragments were also measured. The angle of one of the neutron detectors N_1 relative to the fragments was varied through a range from 22.5 to 90 deg in steps of 11.25 deg. The position of the neutron detector N_2 was held constant at 11.25 deg throughout the series of measurements.

A Cf^{252} source of initial strength 1.56×10^6 spontaneous fissions per min was mounted at the center of the drum. It was prepared on a thin nickel foil (90 $\mu g/cm^2$) by the self-transfer method.[4] The Cf^{252} deposit, collected over a two day period, was essentially weightless and covered an area of 0.3 cm^2.

The four detectors located around the periphery of the drum were mounted on 5-in. photomultipliers, each with its associated fast-slow preamplifier. The slow outputs were used to produce microsecond gate pulses for the slow-coincidence system. The fast outputs, after amplification in wide-band amplifiers, were fed to the time-to-pulse-height converters, whose outputs were in turn temporarily stored until they could be converted serially to digital form. While the binary equivalents of the four pulse heights were being punched onto paper tape in the order F_1, F_2, N_1, and N_2, the slow-coincidence unit was disabled. The data recorded on paper tape were then transferred to magnetic tape in a form that retained the identity of each fission event and was directly acceptable by the IBM 704 and 709 computers.

[4] Raymond C. Gatti, Llad Phillips, Harry R. Bowman, and Stanley G. Thompson, University of California Lawrence Radiation Laboratory Report UCRL-9566, 1960 (unpublished), p. 184.

B. Time-per-Channel Calibrations (S)

With a linear time-to-pulse-height conversion system, time is determined through the relation

$$T=T_0+S\times\text{channel number}.$$

The time per channel S for neutrons and fission fragments was determined before and after each run by means of a nanosecond mercury pulser and three calibrated delay lines used in five combinations ranging from 123 to 285 nsec delay time. These delay cables were calibrated by using the three-scope method, with errors not exceeding ±0.2 nsec.[5] Pulses from the pulser were fed into all five detectors simultaneously and the pulses from the zero-time detector were delayed by means of the various delay lines. Thus, the voltage pulse heights (from the time-to-pulse-height converters) were found as functions of delay time. The values of S determined from each set of calibrations for a given run were constant within 1% for the measurements reported here. The average time per channel was approximately 1.6 nsec.

The constant T_0 is most easily obtained through the use of some radiation of known velocity. In the neutron detector this is conveniently provided by the prompt-fission γ rays, as shown in Fig. 2. Unfortunately there is no convenient radiation for use with the fission detectors. The usual procedure is to determine T_0 by measuring the fragment time-of-flight spectrum at two different distances, one of which is as short as possible. With our apparatus it was difficult to use a short flight path, and therefore T_0 was found by comparison of the fragment time-of-flight spectrum with that from Milton and Fraser.[6] A typical spectrum is shown in Fig. 3.

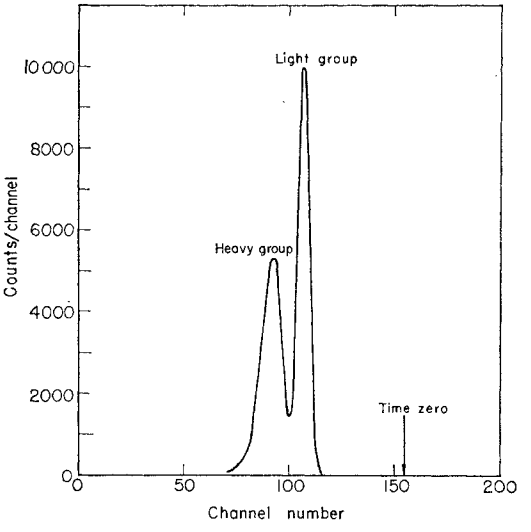

FIG. 3. Time-of-flight spectrum of fission fragments in counter F_1.

[5] This calibration method is described in an internal report of R. C. Epps, University of California Radiation Laboratory, UCID-4300, 1956 (unpublished).

[6] J. C. D. Milton and J. S. Fraser, Phys. Rev. 111, 877 (1958).

C. Measurements of Flight Distance (D), Fission Rate (R), and Solid Angles (ω)

The measured distances from the source to the faces of the detectors were 91.15 cm for neutron detectors N_1 and N_2; 100.0 cm for fission detectors F_1 and F_2.

Since the distance from the fission source to the time-zero detector was 2.9 cm, the distance over which the time was measured for fragments traveling in the direction of counter F_1 was 97.1 cm.

The distance traveled by neutrons also depends on the position in the neutron detector at which a proton recoil is produced. The detectors were 5.08 cm thick and the average scattering position was 2.2 cm from the face. (Calculation of the average scattering position is described in Appendix I.) The values of D used for the distance traveled by neutrons is therefore 93.3 cm. The area of the detectors (πr^2) was 81.07 cm^2. Solid angles ($\pi r^2/D^2$), subtended by the neutron detectors N_1 and N_2, were, therefore, 0.931×10^{-2} sr. The rate of fragment-fragment coincidences (neutrons not in coincidence) was measured periodically. The initial counting rate was 1070 count/min. The decrease in the counting rate over the period of the measurements was within 3% of the decrease expected from the radioactive decay of Cf^{252} (half-life 2.2 years).

D. Operating Procedures and Data-Check System

Before proceeding with analysis of the data it was necessary to use the time-of-flight data recorded on paper tape (Figs. 2 and 3) for the following purposes:

(a) to determine whether the equipment was operating properly during the run (by comparison with data from other runs made under especially good operating conditions);

(b) to make sure of satisfactory time resolution, as indicated for neutrons by the width of the prompt γ-ray peak—normal FWHM (full width at half maximum)=4.0 nsec—and for fission fragments by the general shape and peak-to-valley ratio of the distribution;

(c) to obtain the channel number corresponding to zero time for calculation of velocities;

(d) to determine background corrections for neutrons;

(e) to compare with information transferred onto magnetic tape in order to insure proper operation of data-reduction system.

The information punched on paper tape for each detector system was transferred separately to a pulse-height analyzer and the results printed out to give the number of events recorded in each channel (referred to as a time-of-flight distribution for each one of the four detector systems).

Similar time-of-flight distributions were obtained from the information recorded on magnetic tape by using the magnetic tape as input to the IBM 704 and 709 computers. In this case the computers sorted out the number of events in each channel for each detector system, and the printed output was compared with the "print-out" of the information from paper tape for the same run. Examples of the spectra for neutrons and fission fragments are shown in Figs. 2 and 3. Unless the two print-outs were identical a new magnetic tape record was made and checked.

Occasionally the output from the time-to-height converters was displayed directly on a 400-channel RIDL pulse-height analyzer and used to check the operation of the equipment.

E. Background

Corrections were made for the background of accidental neutrons and γ rays detected by the neutron counters. The magnitude of this background depends on the flux of neutrons and γ rays at the counters and on the length of the coincidence interval.

The background counts are the sums of two components—one that is constant with time, and one that increases roughly linearly with time. The first type results from the usual random coincidences; it is given by $N_f N_n \Delta t$, where N_f is the rate of fission pairs and N_n is the rate in the neutron counter. It may also be estimated from the number of events recorded in channels representing times immediately before fission. The second type stems from neutrons that were associated with the detected fission fragments but had undergone single or multiple scattering before reaching the detector. We may estimate the value of this component from the number of events recorded at the discriminator cutoff (E_n=0.345 Mev). (See point a of Fig. 2.)

Separate experiments were performed to determine the magnitude and functional form of the "scattered" background. For this purpose a shadow cone was placed between the source and the neutron counter; counting rates of accidental events in the time channels were then found to increase linearly as the time after T_0 increased. The standard deviations of the points from a straight line drawn through the group were no more than 5%.

The method of estimating the background is then to join points a and c of Fig. 2 with a straight line. Of course, the background at b should not have a value greater than the height of the distribution at this point. In an average 22-hr run the background per 1.6-nsec time channel at (a) was 6 counts and at (b) was 4. The peak height of the distribution was 400 counts in the same period.

F. Neutron-Detector Efficiencies

The number of neutrons counted in each time channel is dependent not only on the intensity and characteristics of the actual velocity (or energy) spectrum of neutrons from the fission source but also on the detec-

tion efficiency of the plastic detector. Therefore, the number of neutrons counted in each velocity interval was divided by the efficiency of the detector in order to obtain the actual number impinging on the detector.

The efficiencies of the neutron detectors were measured by using a standard Cf^{252} source. This source was standardized as follows: The time-of-flight distribution of neutrons from the standard source was measured by using a thin detector (1 cm thick). Both source and detector were suspended in mid-air, far from any scattering medium. The advantage of a thin detector is that a simple calculation of the efficiency can be made by considering only singly scattered neutrons. The velocity distribution could then be calculated from the known dimensions and composition of the thin detector (density 1.024 g/cm^3; 90.84 wt % C, 8.36% H) and the scattering cross section for hydrogen[7–9] and carbon. This calculated distribution was then compared with the time-of-flight distribution after the subtraction of a background constant in flight time. The total number of neutrons per fission from the Cf^{252} source, obtained by integration of the distribution within the velocity limits of our experiments, was 3.77. This is 10% greater than the value expected within these limits on the basis of the value $\bar{\nu}=3.82$ determined by independent methods[10–12] specifically designed to measure $\bar{\nu}$. The reason for the difference is not known, but may involve the assumptions made in calculating the efficiency of the small detector. Each point on the velocity-distribution curve for the standard source was reduced by 10%.

The efficiencies of the large detectors N_1 and N_2 were then determined by using them to measure the time-of-flight distributions from the standard source inside the steel drum. By removing the background as described in Sec. E, rough accounting was made for the effects of n, n', n, γ, and γ, γ' reactions inside the tank. Any remaining small contribution of these reactions, along with the second-order scattering in the crystal, was taken into account by the efficiency.

The efficiency curve of counter N_1 used in these experiments is shown in Fig. 4. The integrated efficiency of counter N_2 is $3\pm1.5\%$ higher than that of N_1, but the dependence on velocity was the same. A check was made to detect any apparent increase in efficiency due to scattering from the second counter placed in the immediately adjacent position. No effect outside the statistics was found.

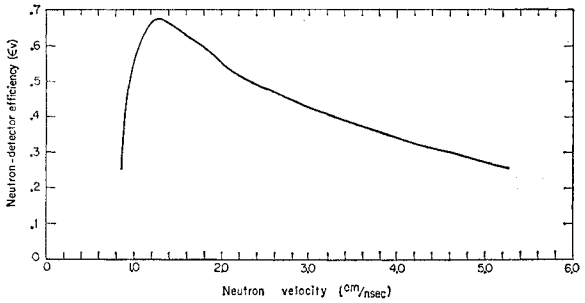

FIG. 4. Detection efficiency ϵ_V for neutron counter N_1 as a function of velocity.

G. Neutron Bias Settings

The neutron bias level was adjusted to the center of the 60-kev γ line from Am^{241}. Such an adjustment was made before and after each run. If the bias level had shifted during the run that run was discarded. The average pulse heights produced by 60-kev γ rays were found to be equal to the maximum pulse height produced in the plastic detectors by neutrons of energy 0.345 ± 0.030 Mev. The corresponding velocity is $V=0.81$ cm/nsec. To be safe, no measurements below $V=1$ cm/nsec were considered in the calculations.

H. Pulse-Height Compensation Network

The major fluctuation in the measurement of neutron time of flight was caused by the variation in pulse height from the neutron detectors. These fluctuations were somewhat reduced by amplifying and limiting the pulses, but the major reduction in timing jitter for neutrons depositing less than 0.8 Mev in the detectors was through the use of a pulse-height compensation network. Since a small pulse activates a time-to-pulse-height converter later than a large pulse even though the rise times are the same, a portion of the slow output from the neutron detectors was mixed with the output of the time-to-pulse-height converters in a manner which minimized the effect.

The optimum conditions for operation of the compensation networks were established by both (a) minimizing the width of the prompt γ-ray distribution (Fig. 2) and (b) using a signal generator to produce two triggering pulses with a fixed time interval between them. The pulses were shaped to have the same characteristics as those occurring during the experiment. The compensation network was adjusted until the output of the time-to-height converter remained constant when the input triggering pulses were varied independently.

I. General Description of the Calculations

The calculations involve quantities defined as follows: D, the average distance traveled by neutrons, over

[7] R. E. Fields, R. L. Becker, and R. K. Adair, Phys. Rev. **94**, 389 (1954).
[8] C. L. Storrs and D. H. Frisch, Phys. Rev. **95**, 1252 (1954).
[9] E. M. Hafner, W. F. Hornyak, C. E. Falk, G. Snow, and T. Coor, Phys. Rev. **89**, 204 (1953).
[10] D. A. Hicks, J. Ise, Jr., and R. V. Pyle, Phys. Rev. **101**, 1016 (1956).
[11] B. C. Diven, H. C. Martin, R. F. Taschek, and J. Terrell, Phys. Rev. **101**, 1012 (1956).
[12] H. R. Bowman and S. G. Thompson, in *Proceedings of the Second United Nations International Conference on the Peaceful Uses of Atomic Energy, Geneva, 1958* (United Nations, Geneva, 1959), Paper P/652 [also Lawrence Radiation Laboratory Report UCRL-5038, 1958 (unpublished)].

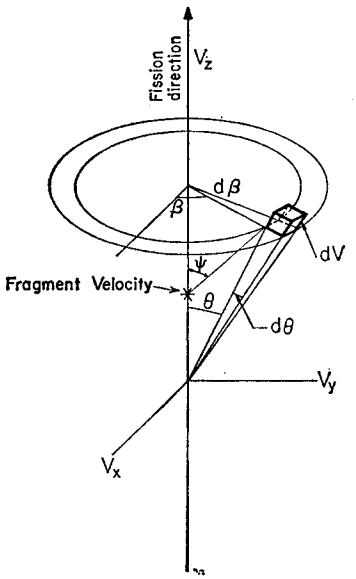

FIG. 5. Schematic representation of the angular relations involved in $\rho(V,\theta)$, where $d\omega=\sin\theta \times d\theta d\beta$ and $d(\text{volume})=V^2 d\omega dV$.

which the flight time is measured; N, the number of neutrons detected in the time interval S; R, the number of fragment-fragment coincidences without reference to neutrons; ω, the solid angle subtended by each of the neutron counters; ϵ_V, the counting efficiency of the detector (Fig. 4); V, the velocity of the neutron appropriate to the center of the time interval S; and θ, the angle relative to the direction of the light fission fragment.

The results have been expressed in terms of the distribution function $\rho(V,\theta)$. The probability per fission that a neutron making an angle θ with the fragment has a velocity V in the interval dV within the solid angle $d\omega$ is $\rho(V,\theta)V^2 dV d\omega$. The values of V, θ, and ω are all determined in the laboratory system. It may be noted by reference to Fig. 5 that $d\omega=\sin\theta d\theta d\beta$. The values of $\rho(V,\theta)$ were computed from the experimental data by means of the equation (derived in Appendix II)

$$\rho(V,\theta)=DN/(R\omega\epsilon V^4 S). \tag{1}$$

In terms of this definition the average number of neutrons per fission $\bar{\nu}$ may be obtained by integrating the density of neutrons per unit volume of velocity space $\rho(V,\theta)$ over all velocities between the velocity limits 0 and ∞, and over all angles θ and β as illustrated in Fig. 5:

$$\bar{\nu}=\int_0^{\pi}\int_0^{\infty}\int_0^{2\pi}\rho(V,\theta)V\sin\theta d\beta dV\, V d\theta,$$
$$\bar{\nu}=2\pi\int_0^{\pi}\int_0^{\infty}\rho(V,\theta)V^2\sin\theta dV d\theta. \tag{2}$$

J. Calculation of the Velocities

The calculations of $\rho(V,\theta)$ were made with IBM 704 and 709 computers using magnetic tape input. Four arrays of 256 channels each were set up:

(1) Counter N_2, light fragment in the direction of F_2;
(2) Counter N_2, heavy fragment in the direction of F_2;
(3) Counter N_1, light fragment in the direction of F_2;
(4) Counter N_1, heavy fragment in the direction of F_2.

The events were then sorted into the appropriate array. In each case it was necessary to calculate the masses of the fragments in order to determine whether a particular event could be assigned to the light or heavy group. The values of $\rho(V,\theta)$ were then readily computed from Eq. (1).

The relation between channel number and velocity, either of fission fragments or neutrons, is

$$V=[D/(T_0-X)S+\Delta t]+\Delta V, \tag{3}$$

where D is the flight path. (In the case of one of the fragments it is measured from the start foil; in the other, from the source. For the neutron it is of course measured from the source.) X is the channel number in which the neutron or fragment is observed, T_0 is the channel number corresponding to time zero, S is the time per channel, Δt is a correction for timing delay (see below), and ΔV is a correction for velocity change of fragments in the nickel foils.

Calculation of the velocity of a neutron or fragment requires knowledge of the velocity of the fragment that traverses the time-zero detector, because of the separation of the source and detector (2.9 cm). However, for the purpose of the $\rho(V,\theta)$ calculation, it is sufficiently accurate to use an average value for the velocity of the appropriate light or heavy fragment in order to make the correction Δt. For calculating the velocity of the fragment passing through the time-zero detector (F_1) the value of Δt is always zero.

The other correction term ΔV is applicable only to the fission fragments. It is zero for calculating the velocities of neutrons. The value of the correction ΔV is found in Appendix III to be 0.015×10^9 cm/sec for both fragments, each of which passes through one foil.

Before being printed out, the four arrays are corrected for background. A run of 15 000 events requires 1 min of computing time on the IBM 709 computer.

K. Corrections

a. *Dead Time of Apparatus*

The dead time of the equipment corresponding to each coincidence event was 365 msec as determined by two methods in excellent agreement. The first used a cathode-ray oscilloscope, and the second a standard, readily identifiable timing pulse injected into the system at regular periods during the actual runs; the dead time was calculated from the number of such pulses found to be missing from the record. The average total dead time during the experiments was about 8%. The correction for dead time was always included in the results of the calculations.

TABLE I. Corrections for fragments lost owing to neutron recoil, calculated as a reciprocal efficiency for the fragment detectors.

θ (deg) \ Neutron velocity [(cm/sec)$\times 10^9$]	0.50	1.00	1.50	2.00	2.50	3.00	3.50	4.00	4.50	5.00
0.00	0.966	0.966	0.966	0.966	0.966	0.966	0.966	0.966	0.966	0.966
11.25	0.966	0.966	0.967	0.968	0.969	0.970	0.972	0.974	0.976	0.978
22.50	0.966	0.968	0.970	0.973	0.978	0.983	0.990	0.998	1.007	1.018
33.75	0.967	0.970	0.975	0.982	0.992	1.004	1.020	1.042	1.068	1.097
45.00	0.967	0.972	0.980	0.993	1.009	1.033	1.065	1.103	1.144	1.191
56.25	0.968	0.975	0.986	1.004	1.030	1.067	1.112	1.163	1.221	1.286
67.50	0.969	0.977	0.991	1.014	1.050	1.096	1.151	1.214	1.286	1.368
78.75	0.969	0.978	0.995	1.021	1.063	1.116	1.177	1.248	1.330	1.424
90.00	0.969	0.979	0.996	1.024	1.068	1.122	1.186	1.260	1.346	1.445

b. *Decay*

The experimental results were obtained over a period of about 6 months, during which time the intensity of the source decreased by about 15%. (The half-life of Cf^{252} is 2.2 years.) Corrections for decay were always made in order to make the results comparable as of the same initial time.

c. *Deflection of Fragments by Neutron Recoil*

In computing the number of neutrons in each velocity interval a correction was made for the deflection of fragments due to recoil by neutrons. In general, after emission of neutrons, the angle between fragments is no longer 180 deg and the probability of detecting both fragments is diminished. The correction is largest for neutron center-of-mass angles close to 90 deg and for high neutron velocities. The correction has been discussed by Milton and Fraser,[6] and in more detail by Milton.[13] Tables of corrections calculated by the method of Milton[13] for the experimental conditions existing in our experiments are given in Table I.

d. *Angular Dispersion*

The correction due to the finite angles subtended by the fission and neutron detectors were computed. The correction is largest where the curvature of $V^2\rho(V,\theta)$ in the θ direction is largest. Thus, the highest value of the correction for the angles of this experiment occurs at large velocities and at 90 deg. For this angle and $V=5.0$ cm/nsec the correction reaches the value of -5%. It is in this region that the velocity dispersion also becomes large, and in fact is very much larger than the angular dispersion. The maximum correction for angular dispersion at 11.25 deg is -1.5% at $V=1.4$ cm/nsec. When $\rho(V,\theta)$ is integrated over all velocities the correction for angular dispersion is negligible, being everywhere less than 1%. Therefore, these corrections were not applied to the final $\rho(V,\theta)$ data.

[13] J. C. D. Milton, University of California Lawrence Radiation Laboratory Report UCRL-9766 (unpublished).

e. *Neutron Velocity Dispersion*

Experimental dispersions in the measurements of neutron velocities arise from:

(a) timing uncertainties inherent in the detection system,

(b) variation in velocities of fragments traveling from the source to the time-zero foil,

(c) the finite width of the time channels,

(d) variation in the distance traveled by neutrons in the neutron detectors, which may be as much as 5 cm, since the proton recoil may occur at any point in the 5 cm thick detector (the average scattering position in the detectors was calculated to be 2.2 cm from the face with a FWHM of 3.0 cm. See Appendix I.)

The total dispersion of (a), (b), and (c) taken together is measured by the width of the prompt γ distribution (approx 4 nsec FWHM). This is the major uncertainty, and it could not be reduced significantly by further amplification of the pulses entering the time-to-pulse-height converters or by optimizing the performance of the associated pulse-height compensation networks.

The total dispersion ΔV is assumed to be given by the relation for uncorrelated Δt and Δx,

$$(\Delta V/V)^2=(\Delta t/t)^2+(\Delta x/D)^2,$$

where Δx is the deviation from the average scattering position in the detector, D is the distance from the source to the average scattering position in the detector, Δt is approximately 4 nsec, t is the time of flight of the particles, and V is the velocity of the particles.

The first term includes the effects of (a), (b), and (c); the second takes care of (d). The dispersion correction was then calculated by folding a Gaussian with width (FWHM) given by ΔV above into an analytical expression for ρ known to fit the experimental data and comparing the results with the value of ρ before folding. The correction so obtained was in turn applied to the measured values.

The influence of velocity dispersion is readily seen by comparing Tables II and III with IV and V.

TABLE II. The neutron densities $[\rho(V,\theta)]$ in neutrons per fission per (cm/nsec)^3 for laboratory velocities and angles relative to the direction of the light fission fragments. Uncorrected for velocity dispersion.

V (10^9 cm/sec) \ θ	11.25°	22.50°	33.75°	45.00°	56.25°	67.50°	78.75°	90.00°
	$100(\rho\pm\Delta\rho)$	$100(\rho\pm\Delta\rho)$	$100(\rho\pm\Delta\rho)$	$100(\rho\pm\Delta\rho)$	$100(\rho\pm\Delta\rho)$	$100(\rho\pm\Delta\rho)$	$100(\rho\pm\Delta\rho)$	$100(\rho\pm\Delta\rho)$
1.025	13.052±0.324	12.431±0.961	12.354±0.972	10.035±0.889	8.074±0.897	7.504±0.739	4.867±0.631	5.946±0.313
1.076	13.386±0.307	15.045±1.023	11.821±0.889	7.589±0.694	10.916±1.021	9.989±0.856	8.852±0.951	6.189±0.309
1.130	13.054±0.283	14.900±0.950	11.494±0.820	9.790±0.773	7.741±0.768	7.562±0.672	6.358±0.724	5.935±0.273
1.186	13.081±0.266	15.144±0.897	13.373±0.847	10.805±0.772	8.209±0.752	8.019±0.661	5.311±0.613	6.034±0.275
1.245	12.832±0.247	13.485±0.788	12.910±0.781	10.131±0.699	7.157±0.656	6.906±0.572	4.535±0.531	4.788±0.226
1.308	13.584±0.241	12.771±0.719	11.879±0.702	8.957±0.616	7.556±0.644	4.960±0.444	4.507±0.508	4.592±0.211
1.373	13.298±0.224	14.429±0.728	13.050±0.701	9.984±0.620	6.215±0.545	5.008±0.426	4.551±0.492	4.256±0.193
1.442	13.892±0.217	14.672±0.693	10.357±0.584	8.884±0.549	6.854±0.550	4.607±0.388	4.241±0.453	3.907±0.175
1.514	14.387±0.209	13.692±0.632	10.796±0.566	7.635±0.479	5.086±0.441	4.441±0.363	3.201±0.365	3.474±0.157
1.590	14.848±0.201	13.499±0.592	10.283±0.522	7.000±0.434	4.928±0.412	3.738±0.313	3.996±0.402	3.069±0.139
1.669	14.980±0.190	12.117±0.528	8.861±0.455	6.327±0.388	5.228±0.406	3.762±0.301	2.824±0.313	2.474±0.117
1.753	14.349±0.176	11.457±0.486	8.548±0.424	6.617±0.378	4.252±0.345	2.651±0.235	2.674±0.291	2.244±0.106
1.840	14.477±0.167	11.205±0.455	8.110±0.392	5.880±0.338	3.703±0.304	2.601±0.222	2.131±0.245	2.008±0.095
1.932	13.878±0.155	10.085±0.410	7.360±0.355	5.038±0.296	3.084±0.263	2.670±0.217	1.774±0.212	1.493±0.077
2.029	12.770±0.141	9.575±0.380	6.474±0.316	4.635±0.271	2.594±0.229	2.070±0.181	1.583±0.191	1.363±0.071
2.131	11.665±0.129	8.274±0.336	5.796±0.285	4.238±0.247	2.559±0.218	1.622±0.151	1.414±0.173	1.235±0.064
2.237	10.293±0.115	7.467±0.303	5.151±0.255	3.633±0.217	1.880±0.177	1.290±0.128	1.103±0.145	0.891±0.051
2.349	8.810±0.100	5.807±0.252	4.689±0.231	2.985±0.186	1.487±0.148	1.419±0.129	0.700±0.106	0.697±0.043
2.467	7.364±0.086	4.785±0.214	3.772±0.194	2.465±0.158	1.421±0.137	0.963±0.099	0.672±0.099	0.621±0.038
2.590	5.785±0.071	3.938±0.182	2.751±0.155	1.964±0.133	1.120±0.114	0.683±0.077	0.531±0.082	0.416±0.029
2.719	4.693±0.060	3.198±0.155	2.206±0.130	1.430±0.106	0.816±0.091	0.609±0.069	0.381±0.065	0.316±0.023
2.855	3.698±0.050	2.355±0.125	1.987±0.117	1.160±0.091	0.623±0.075	0.381±0.050	0.264±0.050	0.273±0.021
2.998	2.726±0.041	1.945±0.107	1.384±0.092	0.808±0.071	0.541±0.066	0.300±0.042	0.247±0.046	0.190±0.016
3.148	2.033±0.033	1.578±0.091	0.976±0.072	0.630±0.059	0.382±0.052	0.210±0.032	0.103±0.025	0.129±0.012
3.306	1.485±0.026	1.130±0.072	0.743±0.059	0.422±0.045	0.293±0.043	0.143±0.025	0.036±0.011	0.089±0.009
3.471	1.022±0.020	0.724±0.054	0.535±0.047	0.272±0.034	0.259±0.038	0.138±0.023	0.049±0.014	0.057±0.006
3.645	0.693±0.016	0.461±0.040	0.358±0.036	0.221±0.029	0.146±0.026	0.087±0.017	0.061±0.016	0.057±0.006
3.827	0.463±0.012	0.366±0.034	0.250±0.028	0.131±0.020	0.114±0.022	0.064±0.013	0.034±0.010	0.048±0.005
4.018	0.302±0.009	0.283±0.029	0.153±0.021	0.095±0.016	0.064±0.014	0.064±0.013	0.034±0.010	0.038±0.004
4.219	0.196±0.007	0.159±0.020	0.089±0.014	0.053±0.011	0.036±0.009	0.056±0.012	0.026±0.008	0.030±0.004
4.430	0.115±0.005	0.122±0.016	0.042±0.008	0.043±0.009	0.032±0.008	0.006±0.002	0.027±0.009	0.023±0.003

TABLE III. The neutron densities $[\rho(V,\theta)]$ in neutrons per fission per (cm/nsec)^3 for laboratory velocities and angles relative to the direction of the heavy fission fragments. Uncorrected for velocity dispersion.

V (10^9 cm/sec) \ θ	168.75°	157.50°	146.25°	135.00°	123.75°	112.50°	101.25°	90.00°
	$100(\rho\pm\Delta\rho)$	$100(\rho\pm\Delta\rho)$	$100(\rho\pm\Delta\rho)$	$100(\rho\pm\Delta\rho)$	$100(\rho\pm\Delta\rho)$	$100(\rho\pm\Delta\rho)$	$100(\rho\pm\Delta\rho)$	$100(\rho\pm\Delta\rho)$
1.025	12.199±0.345	11.433±0.963	6.870±0.664	5.795±0.605	9.501±1.056	7.426±0.745	6.385±0.820	5.838±0.316
1.076	13.243±0.305	10.110±0.788	9.676±0.774	8.665±0.759	7.685±0.805	9.876±0.848	2.881±0.403	6.696±0.326
1.130	12.758±0.279	10.439±0.758	9.458±0.721	11.473±0.852	9.650±0.888	6.802±0.624	7.143±0.784	6.623±0.308
1.186	12.844±0.263	12.067±0.783	9.153±0.668	8.082±0.646	7.263±0.696	5.954±0.545	7.616±0.781	5.129±0.247
1.245	13.172±0.251	11.164±0.704	11.723±0.738	8.397±0.625	8.545±0.730	5.789±0.510	5.757±0.621	5.363±0.243
1.308	12.556±0.230	10.695±0.650	8.917±0.593	7.569±0.557	7.107±0.621	5.605±0.478	5.359±0.569	5.179±0.227
1.373	12.578±0.218	9.687±0.581	8.407±0.546	7.586±0.530	6.644±0.567	4.419±0.394	4.579±0.495	4.600±0.202
1.442	11.968±0.200	10.548±0.578	7.988±0.503	6.974±0.480	5.541±0.486	4.482±0.382	3.601±0.409	4.303±0.186
1.514	11.729±0.187	8.727±0.494	7.158±0.450	6.909±0.454	4.376±0.403	3.595±0.320	3.849±0.409	3.969±0.169
1.590	11.421±0.175	8.656±0.466	7.423±0.436	5.556±0.381	4.381±0.385	3.564±0.305	3.465±0.370	3.278±0.145
1.669	10.764±0.160	8.600±0.440	6.736±0.393	4.776±0.333	4.049±0.351	3.272±0.277	2.615±0.299	2.904±0.129
1.753	10.161±0.147	7.336±0.383	6.015±0.350	5.106±0.328	3.528±0.309	3.077±0.256	2.226±0.261	2.356±0.109
1.840	9.557±0.135	6.780±0.349	5.309±0.312	4.842±0.304	3.400±0.290	2.307±0.208	2.281±0.254	2.038±0.096
1.932	8.472±0.120	6.245±0.318	4.589±0.275	3.711±0.251	2.723±0.245	2.016±0.184	2.096±0.234	1.740±0.084
2.029	7.524±0.107	5.352±0.280	4.612±0.264	3.579±0.236	2.328±0.215	1.515±0.151	1.488±0.184	1.506±0.075
2.131	6.443±0.094	4.575±0.246	3.854±0.229	2.810±0.198	1.909±0.185	1.299±0.133	1.295±0.164	1.274±0.066
2.237	5.531±0.083	4.115±0.222	3.215±0.199	2.438±0.176	1.557±0.159	1.255±0.126	0.726±0.111	0.887±0.051
2.349	4.541±0.071	3.565±0.195	2.776±0.174	1.827±0.143	1.255±0.134	0.879±0.098	0.696±0.105	0.726±0.044
2.467	3.635±0.059	2.768±0.160	2.211±0.146	1.448±0.119	0.863±0.103	0.500±0.066	0.658±0.098	0.592±0.037
2.590	2.837±0.049	2.007±0.127	1.700±0.119	1.249±0.104	0.780±0.092	0.582±0.070	0.263±0.052	0.468±0.031
2.719	2.123±0.040	1.469±0.102	1.166±0.092	0.972±0.086	0.597±0.076	0.362±0.051	0.284±0.053	0.272±0.021
2.855	1.658±0.033	1.111±0.084	0.956±0.079	0.706±0.069	0.393±0.057	0.233±0.037	0.347±0.059	0.226±0.018
2.998	1.164±0.026	0.854±0.069	0.599±0.058	0.502±0.054	0.274±0.044	0.302±0.042	0.258±0.048	0.184±0.015
3.148	0.833±0.020	0.672±0.057	0.477±0.048	0.342±0.042	0.256±0.041	0.188±0.030	0.155±0.033	0.144±0.013
3.306	0.555±0.015	0.380±0.040	0.352±0.039	0.268±0.035	0.147±0.028	0.145±0.025	0.086±0.021	0.107±0.010
3.471	0.389±0.012	0.294±0.033	0.230±0.029	0.160±0.024	0.070±0.016	0.097±0.018	0.043±0.012	0.080±0.008
3.645	0.250±0.009	0.190±0.024	0.103±0.017	0.096±0.017	0.062±0.014	0.072±0.015	0.023±0.007	0.057±0.006
3.827	0.171±0.007	0.132±0.019	0.069±0.012	0.083±0.015	0.022±0.006	0.054±0.012	0.009±0.003	0.034±0.004
4.018	0.113±0.005	0.092±0.014	0.052±0.010	0.022±0.005	0.022±0.006	0.023±0.006	0.000±0.000	0.025±0.003
4.219	0.064±0.003	0.072±0.012	0.030±0.006	0.018±0.005	0.027±0.007	0.027±0.007	0.003±0.001	0.024±0.003
4.430	0.038±0.002	0.024±0.005	0.020±0.005	0.027±0.006	0.023±0.006	0.018±0.005	0.032±0.010	0.022±0.003

TABLE IV. The neutron densities $[\rho(V,\theta)]$ in neutrons per fission per (cm/nsec)^3 for laboratory velocities and angles relative to the direction of the light fission fragments. Corrected for velocity dispersion.

V \ θ (10^9 cm/sec)	11.25°	22.50°	33.75°	45.00°	56.25°	67.50°	78.75°	90.00°
	$100(\rho\pm\Delta\rho)$	$100(\rho\pm\Delta\rho)$	$100(\rho\pm\Delta\rho)$	$100(\rho\pm\Delta\rho)$	$100(\rho\pm\Delta\rho)$	$100(\rho\pm\Delta\rho)$	$100(\rho\pm\Delta\rho)$	$100(\rho\pm\Delta\rho)$
1.025	13.065±0.324	12.430±0.961	12.354±0.972	10.038±0.889	8.078±0.897	7.508±0.739	4.869±0.631	5.895±0.313
1.076	13.394±0.307	15.042±1.023	11.822±0.889	7.592±0.694	10.923±1.021	9.995±0.856	8.857±0.951	6.446±0.309
1.130	13.055±0.283	14.896±0.950	11.495±0.820	9.796±0.773	7.747±0.768	7.567±0.672	6.362±0.724	6.083±0.273
1.186	13.076±0.266	15.139±0.897	13.377±0.847	10.813±0.772	8.217±0.752	8.026±0.661	5.315±0.613	5.586±0.275
1.245	12.805±0.247	13.479±0.788	12.917±0.781	10.141±0.699	7.165±0.656	6.912±0.572	4.539±0.531	5.080±0.226
1.308	13.525±0.241	12.766±0.719	11.890±0.702	8.969±0.616	7.566±0.644	4.965±0.444	4.511±0.508	4.890±0.211
1.373	13.210±0.224	14.424±0.728	13.066±0.701	10.001±0.620	6.224±0.545	5.014±0.426	4.556±0.492	4.433±0.193
1.442	13.805±0.217	14.675±0.693	10.375±0.584	8.901±0.549	6.864±0.550	4.612±0.388	4.246±0.453	4.110±0.175
1.514	14.330±0.209	13.707±0.632	10.822±0.566	7.652±0.479	5.094±0.441	4.448±0.363	3.205±0.365	3.727±0.157
1.590	14.825±0.201	13.526±0.592	10.314±0.522	7.018±0.434	4.937±0.412	3.744±0.313	4.003±0.402	3.179±0.139
1.669	15.004±0.190	12.159±0.528	8.893±0.455	6.343±0.388	5.236±0.406	3.768±0.301	2.829±0.313	2.694±0.117
1.753	14.422±0.176	11.514±0.486	8.583±0.424	6.634±0.378	4.259±0.345	2.655±0.235	2.680±0.291	2.305±0.106
1.840	14.593±0.167	11.275±0.455	8.145±0.392	5.894±0.338	3.709±0.304	2.606±0.222	2.136±0.245	2.028±0.095
1.932	14.019±0.155	10.156±0.410	7.389±0.355	5.047±0.296	3.089±0.263	2.676±0.217	1.779±0.212	1.620±0.077
2.029	12.919±0.141	9.645±0.380	6.495±0.316	4.640±0.271	2.598±0.229	2.075±0.181	1.587±0.191	1.438±0.071
2.131	11.796±0.129	8.324±0.336	5.806±0.285	4.240±0.247	2.564±0.218	1.626±0.151	1.416±0.173	1.256±0.064
2.237	10.391±0.115	7.495±0.303	5.151±0.255	3.633±0.217	1.883±0.177	1.293±0.128	1.104±0.145	0.889±0.051
2.349	8.855±0.100	5.806±0.252	4.678±0.231	2.984±0.186	1.490±0.148	1.421±0.129	0.700±0.106	0.710±0.043
2.467	7.358±0.086	4.764±0.214	3.757±0.194	2.465±0.158	1.424±0.137	0.963±0.099	0.670±0.099	0.603±0.038
2.590	5.737±0.071	3.902±0.182	2.737±0.155	1.965±0.133	1.122±0.114	0.682±0.077	0.527±0.082	0.438±0.029
2.719	4.626±0.060	3.162±0.155	2.197±0.130	1.431±0.106	0.816±0.091	0.606±0.069	0.376±0.065	0.289±0.023
2.855	3.630±0.050	2.327±0.125	1.980±0.117	1.159±0.091	0.620±0.075	0.376±0.050	0.258±0.050	0.242±0.021
2.998	2.674±0.041	1.924±0.107	1.380±0.092	0.806±0.071	0.536±0.066	0.293±0.042	0.238±0.046	0.179±0.016
3.148	1.999±0.033	1.563±0.091	0.970±0.072	0.624±0.059	0.374±0.052	0.202±0.032	0.097±0.025	0.127±0.012
3.306	1.461±0.026	1.116±0.072	0.734±0.059	0.413±0.045	0.282±0.043	0.134±0.025	0.033±0.011	0.088±0.009
3.471	1.003±0.020	0.710±0.054	0.521±0.047	0.262±0.034	0.244±0.038	0.126±0.023	0.043±0.014	0.059±0.006
3.645	0.671±0.016	0.444±0.040	0.341±0.036	0.206±0.029	0.133±0.026	0.076±0.017	0.051±0.016	0.046±0.006
3.827	0.437±0.012	0.342±0.034	0.230±0.028	0.117±0.020	0.098±0.022	0.052±0.013	0.026±0.010	0.030±0.005
4.018	0.274±0.009	0.252±0.029	0.133±0.021	0.079±0.016	0.051±0.014	0.048±0.013	0.023±0.010	0.020±0.004
4.219	0.166±0.007	0.132±0.020	0.071±0.014	0.041±0.011	0.026±0.009	0.037±0.012	0.016±0.008	0.015±0.004
4.430	0.088±0.005	0.091±0.016	0.030±0.008	0.029±0.009	0.020±0.008	0.003±0.002	0.013±0.009	0.010±0.003

TABLE V. The neutron densities $[\rho(V,\theta)]$ in neutrons per fission per (cm/nsec)^3 for laboratory velocities and angles relative to the direction of the heavy fission fragments. Corrected for velocity dispersion.

V \ θ (10^9 cm/sec)	168.75°	157.50°	146.25°	135.00°	123.75°	112.50°	101.25°	90.00°
	$100(\rho\pm\Delta\rho)$	$100(\rho\pm\Delta\rho)$	$100(\rho\pm\Delta\rho)$	$100(\rho\pm\Delta\rho)$	$100(\rho\pm\Delta\rho)$	$100(\rho\pm\Delta\rho)$	$100(\rho\pm\Delta\rho)$	$100(\rho\pm\Delta\rho)$
1.025	12.142±0.345	11.423±0.963	6.870±0.664	5.798±0.605	9.508±1.056	7.431±0.745	6.389±0.820	5.895±0.318
1.076	13.191±0.305	10.103±0.788	9.679±0.774	8.672±0.759	7.692±0.805	9.884±0.848	2.883±0.403	6.446±0.326
1.130	12.716±0.279	10.434±0.758	9.463±0.721	11.484±0.852	9.661±0.888	6.808±0.624	7.149±0.784	6.083±0.308
1.186	12.810±0.263	12.064±0.783	9.161±0.668	8.091±0.646	7.272±0.696	5.960±0.545	7.622±0.781	5.586±0.247
1.245	13.154±0.251	11.169±0.704	11.737±0.738	8.410±0.625	8.557±0.730	5.795±0.510	5.762±0.621	5.080±0.243
1.308	12.558±0.230	10.708±0.650	8.933±0.593	7.582±0.557	7.117±0.621	5.611±0.478	5.364±0.569	4.890±0.227
1.373	12.600±0.218	9.707±0.581	8.426±0.546	7.602±0.530	6.654±0.567	4.424±0.394	4.584±0.495	4.433±0.202
1.442	12.004±0.200	10.578±0.578	8.009±0.503	6.989±0.480	5.549±0.486	4.487±0.382	3.605±0.409	4.110±0.186
1.514	11.780±0.187	8.760±0.494	7.180±0.450	6.924±0.454	4.382±0.403	3.599±0.320	3.853±0.409	3.727±0.169
1.590	10.486±0.175	8.696±0.466	7.449±0.436	5.569±0.381	4.387±0.385	3.567±0.305	3.469±0.370	3.179±0.145
1.669	10.831±0.160	8.641±0.440	6.758±0.393	4.785±0.333	4.053±0.351	3.275±0.277	2.619±0.299	2.694±0.129
1.753	10.229±0.147	7.372±0.383	6.033±0.350	5.112±0.328	3.530±0.309	3.080±0.256	2.230±0.261	2.305±0.109
1.840	9.619±0.135	6.810±0.349	5.321±0.312	4.845±0.304	3.401±0.290	2.310±0.208	2.285±0.254	2.028±0.096
1.932	8.516±0.120	6.263±0.318	4.593±0.275	3.710±0.251	2.723±0.245	2.018±0.184	2.100±0.234	1.620±0.084
2.029	7.549±0.107	5.358±0.280	4.609±0.264	3.575±0.236	2.328±0.215	1.517±0.151	1.491±0.184	1.438±0.075
2.131	6.443±0.094	4.568±0.246	3.845±0.229	2.805±0.198	1.909±0.185	1.301±0.133	1.297±0.164	1.256±0.066
2.237	5.512±0.083	4.098±0.222	3.203±0.199	2.434±0.176	1.558±0.159	1.257±0.126	0.727±0.111	0.889±0.051
2.349	4.509±0.071	3.543±0.195	2.765±0.174	1.825±0.143	1.256±0.134	0.879±0.098	0.696±0.105	0.710±0.044
2.467	3.601±0.059	2.748±0.160	2.202±0.146	1.447±0.119	0.863±0.103	0.500±0.066	0.656±0.098	0.603±0.037
2.590	2.807±0.049	1.992±0.127	1.695±0.119	1.249±0.104	0.780±0.092	0.581±0.070	0.261±0.052	0.438±0.031
2.719	2.104±0.040	1.460±0.102	1.164±0.092	0.971±0.086	0.595±0.076	0.360±0.051	0.279±0.053	0.289±0.021
2.855	1.644±0.033	1.105±0.084	0.953±0.079	0.703±0.069	0.390±0.057	0.230±0.037	0.339±0.059	0.242±0.018
2.998	1.156±0.026	0.849±0.069	0.596±0.058	0.498±0.054	0.270±0.044	0.295±0.042	0.248±0.048	0.179±0.015
3.148	0.824±0.020	0.665±0.057	0.470±0.048	0.335±0.042	0.248±0.041	0.180±0.030	0.145±0.033	0.127±0.013
3.306	0.545±0.015	0.372±0.040	0.342±0.039	0.258±0.035	0.140±0.028	0.135±0.025	0.079±0.021	0.088±0.010
3.471	0.375±0.012	0.283±0.033	0.219±0.029	0.150±0.024	0.064±0.016	0.088±0.018	0.038±0.012	0.059±0.008
3.645	0.235±0.009	0.177±0.024	0.095±0.017	0.087±0.017	0.055±0.014	0.062±0.015	0.019±0.007	0.046±0.006
3.827	0.154±0.007	0.118±0.019	0.060±0.012	0.071±0.015	0.019±0.006	0.043±0.012	0.006±0.003	0.030±0.004
4.018	0.096±0.005	0.077±0.014	0.043±0.010	0.017±0.005	0.017±0.006	0.016±0.006	0.004±0.000	0.020±0.003
4.219	0.049±0.003	0.055±0.012	0.022±0.006	0.013±0.005	0.018±0.007	0.017±0.007	0.002±0.001	0.015±0.003
4.430	0.026±0.002	0.016±0.005	0.013±0.005	0.016±0.006	0.013±0.006	0.009±0.005	0.015±0.010	0.010±0.003

f. *Fission-Fragment Velocity Dispersion*

In calculating center-of-mass spectra, the fragment velocities used were taken to be average velocities of the light and heavy groups. Actually, these groups have velocity distributions with FWHM$=0.15\times10^9$ cm/sec.[6] If, as assumed, the neutrons are evaporated from fully accelerated fragments, the dispersions in fragment velocities produce a dispersion in the observed data. It was found that the error made by neglecting this correction was always less than 1%.

L. Normalization

In a set of 30 runs made under especially good operating conditions the counting rate of counter N_2 and the ratio of counting rates for counter N_2 relative to N_1 were determined. In many of the other runs the data-recording system (Fridén paper punch) failed part of the time and the actual running time could not be determined. In such cases the counting rate of counter N_2 determined under best conditions in its usual 11.25-deg position was chosen as a standard for normalization of the results obtained by counter N_1. $\langle N_2\rangle$ is thus used as an internal clock. The procedure used was as follows:

(1) The correct average rate $\langle N_2\rangle$ was determined from the standard set of runs.

(2) The counting rate of counter N_1 was adjusted so that N_1 (normalized)$=[\langle N_2\rangle/N_2$ (observed)$]\times N_1$ (observed).

M. Preparation of Composite $\rho(V,\theta)$ vs V Curves

Many runs were made at each angle. Because the time calibrations were not always the same for all runs, it was difficult to display their sum on a single curve of $\rho(V,\theta)$. Therefore, a method of making a single composite curve for all runs at the same angle was developed. This method enables one to obtain by interpolation the average value of ρ_i at the center of predetermined velocity channel V_i of width ΔV_i. The over-all statistical error of the average value was also found.

III. RESULTS AND DISCUSSION

The neutron density $\rho(V,\theta)$ as determined in this experiment is presented in Tables II through V and in Figs. 6 and 7. The tabular results have been given both before and after correcting for resolution, since this is probably the most uncertain of all the corrections. Two sections through $\rho(V,\theta)$, taken at lab angles of 11.25 deg and 168.75 deg, are given in Fig. 8, which also shows a plot of the background. (In Fig. 14 we illustrate the lab neutron spectrum averaged over all angles.)

The measured angular distribution of the neutrons in the laboratory system is shown in Fig. 9. The distribution of the neutrons as functions of both angle and velocity is given in Fig. 10 in terms of the density $\rho(V,\theta)$. A visual examination of this figure suggests at once that the over-all features of the neutron distributions associated with californium fission are consistent with approximately isotropic emission from two moving fragments. Thus, the general appearance of Fig. 10, with the lines of constant ρ in the form of elongated ovals, suggests that the neutrons have been emitted from two sources moving in opposite directions with velocities about the same as those of the fragments. (This was shown many years ago by Fraser[14] for the case of thermal-neutron fission.)

The value of a plot such as Fig. 10 lies in the ease with which the hypothesis of isotropic emission of the neutrons from moving fragments may be tested by a graphical construction. Thus, by placing the point of a compass on the point corresponding to the velocity of the light fragment and drawing circles that fit approximately arcs of the $\rho(V,\theta)$ contours in the region of small or moderate angles (where the neutrons from

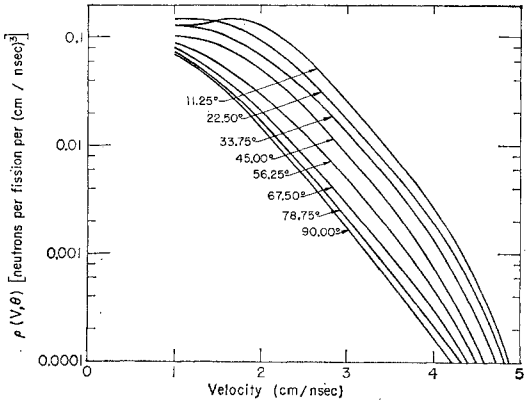

FIG. 6. Neutron density distribution $\rho(V,\theta)$ (lab) as a function of neutron velocity and angle relative to the direction of light fission fragments (corrected for dispersion).

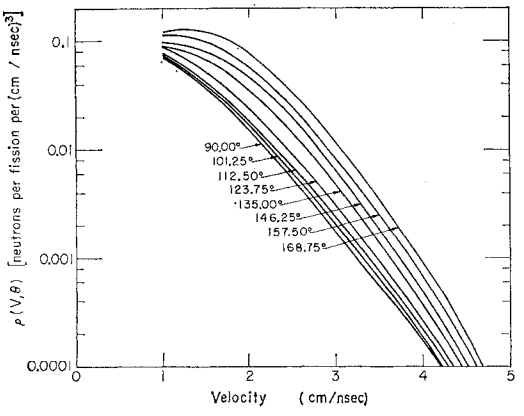

FIG. 7. Neutron density distribution $\rho(V,\theta)$ (lab) as a function of neutron velocity and angle relative to the direction of light fission fragments (corrected for dispersion). The heavy fragment direction corresponds to 180 deg.

[14] J. S. Fraser, Phys. Rev. 88, 536 (1952).

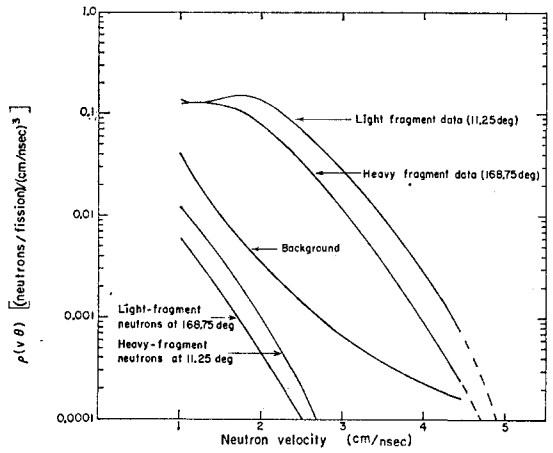

FIG. 8. Neutron density distribution $\rho(V,\theta)$ (lab) (background subtracted) as a function of neutron velocity for light fragments (11.25 deg) and heavy fragments (168.75 deg). Contributions to $\rho(V,\theta)$ from neutrons emitted in the backward direction from opposite fragments are shown along with a typical background distribution.

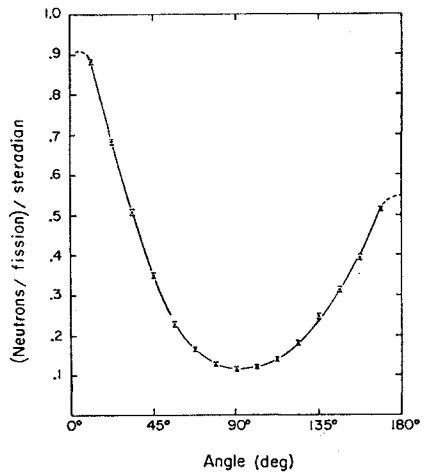

FIG. 9. The measured angular distribution (lab) of neutrons from Cf^{252}.

the heavy fragment are negligible), one obtains the distribution of neutrons that would have come from the light fragment if isotropic emission were valid. Similar circles drawn around the point on the right of the origin in Fig. 10 give the contribution from the heavy fragment. If these circles are imagined as labeled with their appropriate ρ values, the intersection of two circles gives the location where the expected value is the sum of the two labels. In this way a ρ plot corresponding to isotropic emission from moving fragments is obtained and may be compared with the experimental one.

Such a graphical construction confirms the impression that the bulk of the neutrons in Cf fission could be accounted for by isotropic evaporation from moving fragments but even at this stage one becomes aware of small deviations from such a picture. The deviations appear to be of a rather complicated kind, suggesting an excess of neutrons at and around 90 deg to the fission direction as well as an anomalously high number of neutrons at the two angles of 11.25 and 168.75 deg.

In order to test the hypothesis of isotropic evaporation of neutrons from moving fragments quantitatively, and in order to bring out the nature of the deviations, a more refined analysis of the data was carried out.

The principle of the method was to represent the over-all features of the data by simple analytic expressions corresponding to the hypothesis of the emission of neutrons from moving fragments, and to discuss the data in terms of the fits that could be achieved to such expressions. The neutron distributions were assumed to be given by a superposition of contributions from the light and heavy fragments

$$\rho(V,\theta)=\rho_L+\rho_H,$$

where ρ_L and ρ_H are analytic functions of the neutron velocities in the fragment's frames of reference, specified by a number of adjustable parameters. These functions were taken to be superpositions of evaporation spectra[15,16]

$$\phi(\eta)\propto(\eta/T_i^2)\exp(-\eta/T_i),$$

each component in the superposition being characterized by its temperature T_i and its relative weight α_i. The symbol η represents the neutron energy in the center-of-mass system.

Up to three components were necessary to describe adequately the energy dependence of the neutrons over the range of velocities from 1 to 5 cm/nsec. The nature of the energy distributions to be fitted by the superposition of evaporation components is illustrated in Fig. 11, where the neutron spectra from the light and heavy fragments, as deduced from measurements at 11.25 and 168.75 deg, are shown. The measurements in Fig. 11 have been plotted in such a way that a pure evaporation spectrum with a single temperature would appear as a straight line; it is clear that the observed spectra require the superposition of several evaporation components at different temperatures. It should be pointed out that the only assumption involved in Fig. 11 is that the neutrons arise from the moving fragments.

A notable feature of Fig. 11 is the virtual identity of the energy spectra of neutrons from the light and heavy fragments, extending over almost four decades of neutron intensity. This remarkable correspondence of the spectra has made it possible to use the same set of α's and T's to represent the neutrons from the light and heavy fragments, thus halving the number of parameters in the analytic functions ρ_L and ρ_H.

As a refinement, the possibility of a dependence of

[15] J. Terrell, Phys. Rev. 113, 527 (1959).
[16] J. M. Blatt and V. Weisskopf, *Theoretical Nuclear Physics* (John Wiley & Sons, Inc., New York, 1952), p. 365.

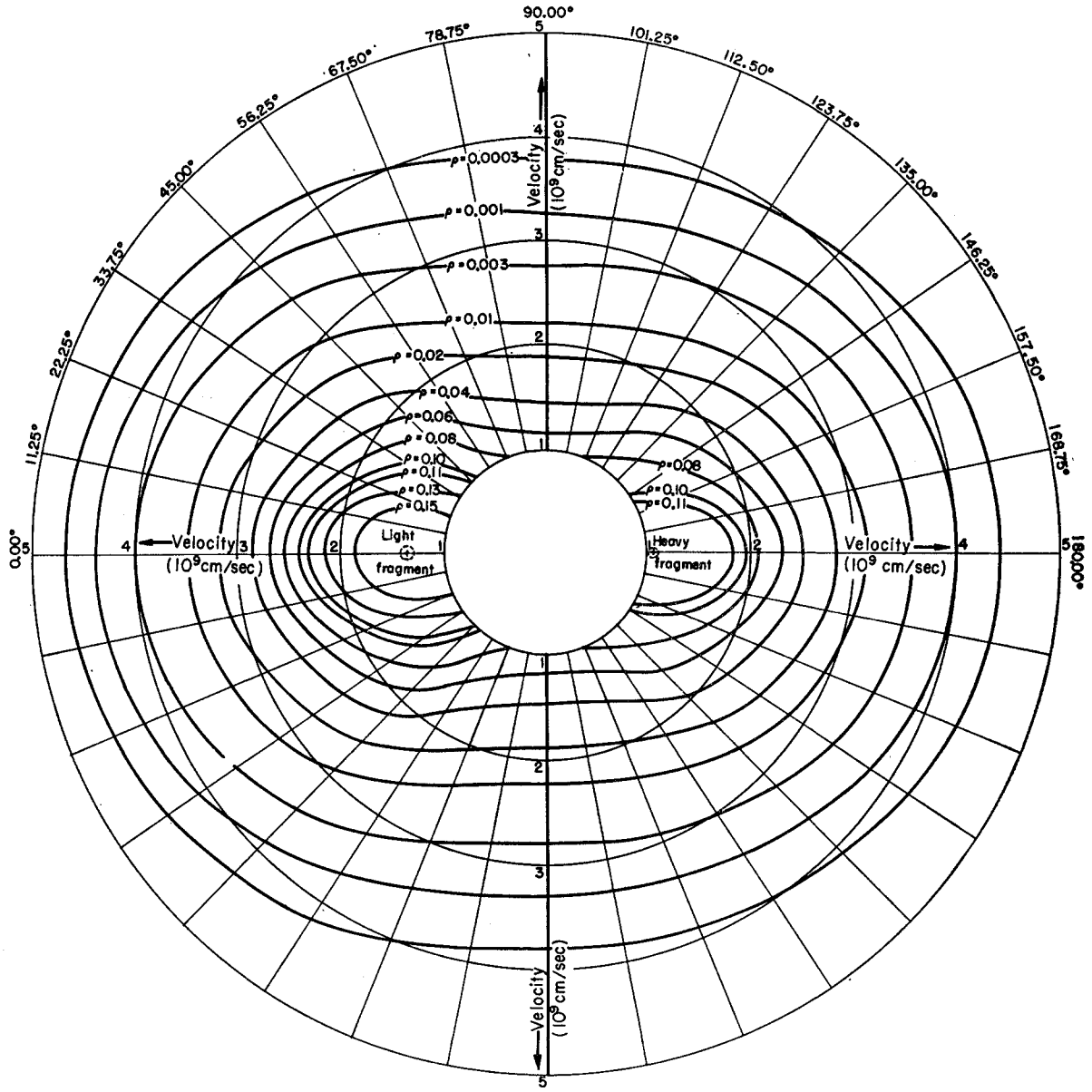

FIG. 10. The contour diagram in polar coordinates of observed neutron density distribution $\rho(V,\theta)$ as a function of neutron velocity and angle. The contour lines are lines of constant neutron density. The average velocities of the light and heavy fission fragments are also shown.

ρ_L and ρ_H on the angle ψ between the neutron and the fragment in the center-of-mass system was allowed for through a factor of the type $1+A_2P_2(\cos\psi)$ using the same A_2 for both fragments. Positive deviations from isotropy of a few percent might be consistent with the hypothesis of neutron evaporation if the neutrons were emitted from fragments possessing large angular momenta—see Ericson and Strutinski.[17]

With the α's, T's, and A_2 as adjustable parameters, the sum of ρ_L and ρ_H was then fitted to the observed neutron distributions by using a slightly modified version of an iterative least-squares program developed in Los Alamos by Moore and Zeigler[18] for an IBM 704 computer. The code name MISFIT was given locally to this program. Further details of the formulas used in the fit are given in Appendix IV.

The method used is that of Gauss, and despite some unexplained aberrations worked surprisingly well in

[17] T. Ericson and V. Strutinski, Nuclear Phys. 8, 284 (1958) with errata 9, 689 (1958/59).

[18] R. H. Moore and R. K. Zeigler, Los Alamos Report 2367, 1960 (unpublished).

TABLE VI. Values obtained for parameters of formulas in Appendix IV by MISFIT program for least-squares fit of data.[a]

Description	S^2	T	α		$\langle T\rangle$	σ_T	A_2	ν_L	ν_L/ν_H
All points	6.60	0.9941	0.3729	0.0731	0.7217	0.316	≡0	1.97±0.01	1.16±0.01
		0.5720	0.4061	0.0219				1.70±0.01	
All points	6.59	0.9906	0.3682	0.0699	0.7214	0.316	0.016±0.012	1.96±0.02	1.16±0.01
		0.5774	0.4020	0.0206				1.69±0.02	
All points	10.30	0.2389	0.8729	...	0.7100	0.277	≡0	1.98±0.02	1.17
		0.2570	0.7430	...				1.68±0.02	
All points	10.29	0.2404	0.8738	...	0.7102	0.277	−0.015±0.014	1.99±0.02	1.17
		0.2583	0.7417	...				1.70±0.02	
Only 11.25 deg	7.71	0.9110	0.3113	0.0544	0.689		≡0	≡1.95	≡1.14
		0.6339	0.3574	0.0087				≡1.72	
Only 168.75 deg	2.04	0.9673	0.3810	0.0508	0.692		≡0		
		0.5436	0.4399	0.0165					
Excluding 11.25 and 168.75 deg	3.92	1.6883	0.7765	0.2280	0.7835	0.376	≡0	1.98±0.02	1.25
		0.1093	0.7217	0.1690				1.58±0.02	
Only 11.25 and 168.75 deg	8.90	0.9266	0.3311	0.0461	0.6923	0.295	≡0	1.95±0.02	1.14
		0.6112	0.3790	0.0098				1.72±0.02	

[a] The quantities T_i, α_i, $\langle T\rangle$, σ_T, A_2, ν_L, and ν_H are defined in the text and in Appendix IV. Their units are specified in Appendix IV. It can be shown that S^2 follows a χ^2 distribution with f degrees of freedom, where f=number of points−number of parameters. See, e.g., A. Hald, *Statistical Theory With Engineering Application* (John Wiley & Sons, Inc., New York, 1952), p. 551. Except for entries 5, 6, 7, and 8, f is in our case approximately 450; hence the probability of obtaining S^2 values as different from unity as these are, is vanishingly small if the ρ samples were derived from the assumed population. In this sense the fits must be considered poor. This is another way of stating that the deviations observed in Fig. 12 are systematic rather than random.

fitting as many as eight parameters to as many as 465 data points. In general the procedure would not converge unless the starting values were rather close to the final ones. However, there were a few notable exceptions in which it successfully converged from starting values very different from the final ones, giving us some confidence that we had not missed any solutions.

More than 25 fits to the data were successfully made. In this way it was rather easy to see how the results were affected by changes in the background, the efficiency, and the resolution correction. In addition, the influence of holding fixed some of the parameters or of introducing additional ones was quickly assessed.

The results of some of the fits are shown in Table VI. The temperatures and relative weights of the component evaporation spectra are given in column 3. As was remarked earlier, a simple evaporation spectrum with one temperature would not be adequate to represent the data. This is to be expected, since in the de-excitation of fission fragments the temperature is not a constant, both on account of the rather wide range of initial excitation energies of the fragments and on account of the decrease in excitation energy in the course of the emission of successive neutrons. The three temperatures in column 3 of Table VI should not, of course, be associated directly with the first, second, or third neutron emitted by a fragment. The list of α and T values represent a first step towards an experimental determination of a temperature distribution $\alpha(T)$ of the type studied by Terrell.[15] The comparison with such a continuous distribution is perhaps best made in terms of quantities like the average temperature $\langle T\rangle$ and the variance σ_T^2. These quantities are listed in columns 4 and 5 of Table VI. The last two columns in Table VI refer to the absolute and relative numbers of neutrons emitted by the two fragments.

In the first line of Table VI the anisotropy parameter A_2 was assumed to be zero. The second line, with A_2 free to vary, shows that no large anisotropy is called for by the data, though a slight anisotropy is consistent with the observations.

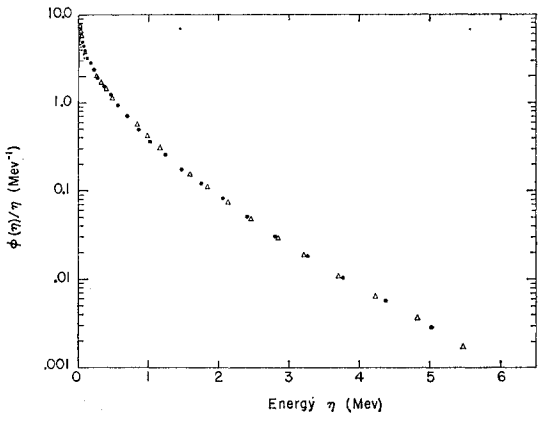

FIG. 11. The center-of-mass neutron energy spectrum $\phi(\eta)$ (c.m.) divided by η. The large dots represent the neutrons emitted in the direction of the light fragments and the triangles represent the neutrons emitted in the direction of the heavy fragments. The smaller dots were obtained from measured neutrons emitted in the backward direction from the light fragments. The curve for light fragments was reduced by the factor 1.16, which is the ratio of the number of neutrons from the light fragments to the number from the heavy fragments.

Line 3 shows the effect of assuming only two components in the energy spectra ρ_L and ρ_H. Comparison with line 1 shows that although the over-all fit is not as good, the optimum values of the parameters $\langle T\rangle$, σ_T, ν_L, and ν_H deduced from the data are not sensitive to the assumption of a third component in the energy spectra.

Lines 5 and 6 in Table VI are given to illustrate the remarkable similarity between the energy spectra of the neutrons emitted by the light and heavy fragments. The numbers of neutrons emitted by the two fragments were taken as in line 8, but the energy spectra were determined by using first the data at 11.25 deg and then the data at 168.75 deg. The resulting values of $\langle T\rangle$ and σ_T are almost identical.

Lines 7 and 8 in Table VI refer to least-squares fits made by using two portions of the data, one at a time. They give some indication of the degree of inconsistency of the data with the hypothesis of isotropic emission from moving fragments. Thus, if all the data were consistent with this hypothesis, the use of different portions of the data should lead, within statistics, to the same parameters. In fact, however, significant differences are observed.

In order to bring out the nature of the differences more directly an analysis was carried out in which deviations from the analytical fits were plotted as functions of angle. A general method was developed for comparing different moments of the observed neutron distributions at different angles with the corresponding moments deduced from an analytical fit. The zeroth moment compares the observed and calculated numbers of neutrons at different angles, the first moment compares the average velocities, the second the average energies. Provisions were made for calculating up to the fourth moment of the distributions. In this manner a rather detailed and yet compact way of analyzing the large amount of data was achieved. This method was used to advantage in bringing out the details of the fine structure in the neutron distributions even before the least-squares fits were available. The observed zeroth, first, and second moments (corrected for dispersion) for all angles are given in Table VII.

Figures 12(a), (b), and (c) show a comparison at each angle from 11.25 to 168.75 deg of the measured number of neutrons and their average velocities and energies with the same quantities calculated from the least-squares solution given by line 1 in Table VI. It will be seen that although the calculated distribution represents the measurements to within 10 to 20%, there seem to be systematic deviations outside of statistical errors. Similar comparisons using other values of the parameters in the calculated distributions, including A_2 values in the range between -1 and $+1$, showed that it was not possible to reduce the deviations at all angles simultaneously. Leaving aside the two points at 11.25 and 168.75 deg, which will be discussed presently, there appears to be a systematic rise in the observed number of neutrons as one approaches the 90-deg direction. The presence of this "bulge," whose maximum amplitude in Fig. 12(a) is about 30%, suggests an analysis in which a fraction of the neutrons, rather than being emitted from moving fragments, is assumed to be emitted isotropically in the laboratory system. Figures 13(a), (b), and (c) show a comparison of the observed distributions with a calculation in which 90% of the neutrons came from the moving fragments (with relative angular and energy distributions the same as in Fig. 12) and 10% were distributed isotropically in the laboratory system with an average energy of 2.6 Mev and an average velocity of 2.11 cm/nsec in the laboratory system. It is clear that the additional freedom introduced into the calculated distributions by the third source of neutrons, at rest in the laboratory system, is of a kind to make possible the removal of

TABLE VII. Measured moments of the neutron distributions (corrected for dispersions).

Angle θ (deg)	Zeroth	First	Second
11.25	0.8864±0.003	2.292±0.002	5.734±0.010
22.50	0.6843±0.007	2.229±0.007	5.497±0.035
33.75	0.5071±0.006	2.181±0.008	5.261±0.039
45.00	0.3507±0.005	2.119±0.009	4.972±0.045
56.25	0.2290±0.004	2.069±0.014	4.813±0.065
67.50	0.1682±0.003	1.990±0.013	4.466±0.063
78.75	0.1270±0.003	1.912±0.012	4.096±0.058
90.00	0.1198±0.001	1.908±0.005	4.102±0.024
101.25	0.1216±0.003	1.870±0.016	3.895±0.073
112.50	0.1407±0.003	1.929±0.014	4.204±0.064
123.75	0.1822±0.004	1.920±0.013	4.110±0.060
135.00	0.2503±0.004	2.016±0.010	4.497±0.047
146.25	0.3141±0.004	2.052±0.009	4.632±0.041
157.50	0.3914±0.005	2.083±0.008	4.793±0.039
168.75	0.5169±0.002	2.104±0.002	4.864±0.011

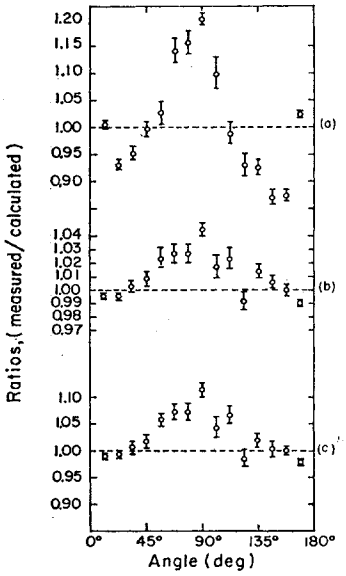

FIG. 12. The ratio of measured to calculated values for (a) numbers of neutrons, (b) average velocities, and (c) average energies as a function of angle. The calculated values were obtained by using a three-temperature-evaporation formula (Appendix IV).

the "bulge" around 90 deg. Moreover, by giving the "third-source" neutrons a relatively high energy (about twice the average energy of the evaporation neutrons, equal to 1.44 Mev), it is possible at the same time to remove the 90-deg bulges in the velocity and energy plots in Figs. 12(b) and (c). There is in fact enough freedom in the calculated distribution to make the fit with observations complete (excepting always the points at 11.25 and 168.75 deg). Thus, the deviation around 135 deg in Fig. 13(a) could be removed by reducing the calculated number of neutrons emitted by the heavy fragment by 10%, to $\nu_H=1.53$ (making $\nu_L/\nu_H=1.29$).

The remaining deviation at 11.25 and 168.75 deg in Figs. 12(a) and 13(a) depend entirely on one counter (the N_2) and its associated electronics (the points at all other angles are associated with one and the same counter, the N_1). Although the average efficiencies of the two systems were found to agree very well, the comparisons depend mainly on measurements made outside the tank and were carried out over a period of time short compared with the duration of the experiment. It is therefore not possible to exclude rigorously a systematic difference between the two counter systems as the reason for the deviations at 11.25 and 168.75 deg. On the other hand, the deviations are rather larger than we would expect in view of the care taken in selecting and comparing the detectors (see Sec. II F), and it seems possible that the effect is a real one. If that is the case it would imply a mechanism for neutron emission, other than evaporation, capable of producing neutrons sufficiently well collimated along the fission direction to affect the counting rates around 11 deg but not significantly around 22 deg in the laboratory system.

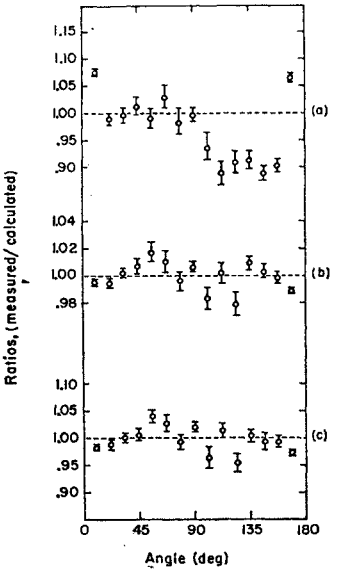

FIG. 13. The ratio of measured to calculated values for (a) numbers of neutrons, (b) average velocities, and (c) average energies as a function of angle when 10% of the total number of neutrons are assumed to come from scission (not evaporated from fragments).

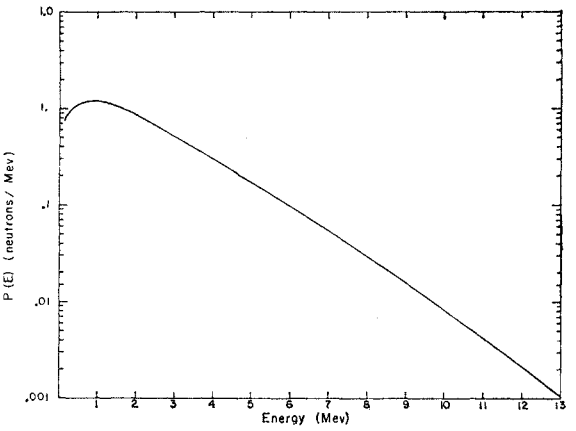

FIG. 14. Energy spectrum in the laboratory system for Cf^{252}. The spectrum is calculated from the parameters of line 1, Table VI, and consequently sums to 3.67 neutrons per fission.

These two small angle points are mainly responsible for the high values of S^2 found in Table VI and since the values are so large it might be argued that the conclusions about the smallness of the anisotropy parameter A_2 are invalid. If these two points are omitted from the fit, S^2 drops to 3.92 (see line 7 of Table VI) but is not further decreased by allowing A_2 to vary, while the value of A_2 called for is still essentially zero. Thus, even without the two small angle points, the remaining deviations are not of such character that they can be reduced by the A_2 term.

We might summarize the results of this experiment by saying that the attempt to interpret the neutrons from Cf^{252} in terms of evaporation from moving fragments succeeds rather well, although not more than about 90% of the neutrons can be accounted for in this way. The evaporation of neutrons from moving fragments provides an immediate explanation of the strong angular anisotropy in Fig. 9, while the value $\langle T\rangle=0.72$ Mev for the temperature of the evaporated neutrons fits in with what is known about nuclear level densities (see, for example, Terrell[15]). On the other hand, we might note in passing that there appears to be some difficulty in attempting to reconcile quantitatively the somewhat greater number of neutrons emitted by the light fragment with the near identity of the temperatures of the light and heavy fragments. For instance, if we assume for the moment that all the neutrons arise from the fragments, then from Table VI we see $\nu_L=1.97$, $\nu_H=1.70$ with $\nu_L/\nu_H=1.16\pm0.01$. The ratio of the excitation energy of the light to the heavy fragment implied by this result is larger than $\nu_L:\nu_H$ because the average neutron binding energy of a light fragment is higher than that of a heavy fragment. This is simply a consequence of the decreasing stability of heavier nuclei in the periodic table. For example, a simple liquid drop formula for nuclear masses predicts the neutron binding energy of average light fragments to be about 5.7 Mev and of average heavy fragments

about 4.7 Mev. (A calculation based on Cameron's[19] masses, in which shell effects are taken into account, gives almost identical average binding energies.)

Taking the average kinetic energies of the neutrons as $2\langle T\rangle = 1.44$ Mev, this gives $1.97(5.7+1.44)=14.1$ Mev for the excitation energy associated with the neutrons emitted by the light fragment and $1.70(4.7+1.44)=10.4$ Mev associated with the neutrons emitted by the heavy fragment. If we assume that the excitation energy of each fragment is 4.5 Mev higher than the above figures to allow for the 9 Mev emitted as γ rays we find the ratio of excitation in the light to that in the heavy fragments to be $(14.1+4.5)/(10.4+4.5)=1.26$. The ratio of the internal excitations per particle (related to the temperatures) would then be $1.26(142/107)=1.67$ indicating that the light fragment should be "hotter" by an appreciable amount (by about 30% if the temperature is taken to be proportional to the square root of the excitation energy per particle). The detection of such a difference is within the precision of this experiment, but, as seen from Fig. 11 and Table VI, the difference has not in fact been observed. The superposition of shell effects on the simple theory (see for example Cameron),[20] although in the right direction, does not appear to be sufficient to eliminate the discrepancy, unless the heavy fragment emits 3 to 4 Mev more γ-ray energy than the light. The shell corrections result in the light and heavy fragments having the same temperature at equal excitation energies.

The observation of deviations from the hypothesis of isotropic evaporation of neutrons from moving fragments, discussed in connection with Figs. 12 and 13, is, from a theoretical point of view, not surprising. The rather violent disturbances associated with the snapping of the neck at the moment of scission (see, for example, Halpern[21]) and the retraction of the stumps into the fragments might well be responsible for the emission of a fraction of the neutrons observed in fission. This possibility was in fact suggested in the classic paper of Bohr and Wheeler from which we quote the relevant paragraph:

"We consider briefly the third possibility that the neutrons in question are produced during the fission process itself. In this connection attention may be called to observations on the manner in which a fluid mass of unstable form divides into two smaller masses of greater stability; it is found that tiny droplets are generally formed in the space where the original enveloping surface was torn apart. Although a detailed dynamical account of the division process will be even more complicated for a nucleus than for a fluid mass, the liquid drop model of the nucleus suggests that it is not unreasonable to expect at the moment of fission a production of neutrons from the nucleus analogous to the creation of the droplets from the fluid."

Attempts to make estimates of such processes have been reported by Fuller[22] and Stavinsky.[23]

If the deviations from the hypothesis of isotropic evaporation found in this experiment are indeed related to neutrons emitted in the very short time during and just after scission, a detailed study of such neutrons, carrying information on the unusual conditions of nuclear matter during the breaking apart of the fission fragments, might well be worth while. It will be clear, however, from the relative smallness of the effects involved, that future experiments would have to aim at a determination of the neutron distributions with a precision of the order of 1 or 2%. Our experiment suggests also the need for very careful measurements of the neutron intensities at small angles, in order to confirm or disprove the presence of a narrow bundle of neutrons along the fission direction. Some further light on these processes may be shed by the more refined analysis, now in progress, of the data of this experiment, in which the correlation of the neutron distributions with the masses and energies of the fragments is taken into account.

SUMMARY

The Characteristics of the Neutrons Emitted in the Spontaneous Fission of Cf^{252}

A. The over-all properties of the neutrons are as follows:

(1) The number of neutrons per fission is $\bar{\nu}=3.8$ (see references 10–12).

(2) The energy spectrum is a rapidly decreasing one, with an average energy 2.34 ± 0.05 Mev and root mean square deviation (width) of 1.73 ± 0.03 Mev in the laboratory system.

(3) The angular distribution is strongly peaked in the direction of the fission fragments: the relative intensities in the direction of the light fragment, in the direction of the heavy fragment and at right angles are about 9, 5, and 1, respectively.

(4) The broad features of the energy and angular distributions are reproduced by the assumption of isotropic evaporation of the neutrons from fully accelerated fragments.

B. If the data are analyzed on the basis of isotropic evaporation from fully accelerated fragments, then:

(5) The light and heavy fragments emit comparable numbers of neutrons with virtually identical energy spectra. An average energy in the center-of-mass system of 1.44 ± 0.08 Mev and rms deviation (width) of 1.28 Mev are calculated from the fitted evaporation spectrum. These correspond to an average temperature of 0.72 ± 0.04 Mev and rms deviation (width) $\sigma_T=0.32$ Mev for each fragment.

[19] A. G. W. Cameron, Can. J. Phys. **35**, 1021 (1957).
[20] A. G. W. Cameron, Can. J. Phys. **36**, 1040 (1958).
[21] I. Halpern, University of Washington Cyclotron Project Progress Report, 1961 (unpublished), p. 921.
[22] R. W. Fuller, thesis, Princeton University, Technical Report NYO-2962, 1961 (unpublished).
[23] V. S. Stavinsky, Soviet Phys.—JETP **36**, 437 (1959).

(6) The light fragment emits 1.97 neutrons, the heavy 1.70 neutrons ($\nu_L/\nu_H=1.16$), which represent contributions to the internal excitation energies of 14.7 Mev and 10.7 Mev, respectively.

(7) The observed deviations from the hypothesis of isotropic emission by fully accelerated fragments are such that not more than about 90% of the neutrons can arise from simple isotropic evaporation.

C. The nature of the deviations is less well determined than the over-all features of the neutron distributions. The following features are suggested:

(8) There is no indication of a marked anisotropy of the $P_2(\cos\psi)$ type in the emission of the neutrons from the fragments.

(9) Most of the systematic deviations from the hypothesis of isotropic emission from moving fragments could be accounted for by assuming a small fraction (for example 10%) of rather energetic neutrons emitted isotropically from a source not sharing the motion of the fragments.

(10) The remaining observed deviations appear at the single small-angle settings (11.25 and 168.75 deg) and would require for their explanation either a small number of neutrons collimated along the fission direction or an unknown instrumental difference in the efficiencies of the two neutron counter systems used in the experiment.

ACKNOWLEDGMENTS

We wish to thank especially Llad Phillips, Raymond Gatti, Richard Martin, Jean Rees, and Arlene Fregulia for their extremely valuable help in all phases of the experiments, which included operation of the equipment, handling and checking the data, making calculations, and helping with the preparation of this report.

The aid of Melvin Brown in connection with the design and construction of electronic equipment and with operations during the course of the experiments is gratefully acknowledged. Further, we wish to thank Elwood Douglas for his efforts in connection with the equipment and operations involved in transferring the data from paper tape to magnetic tape. We are also grateful to Leonard Gibson and Michiyuki Nakamura for their helpful assistance with the electronic equipment involved in the experiments.

The early experiments and construction of much of the apparatus for the last series of experiments was supported by the Livermore laboratory. In this connection we are grateful to Dr. Kenneth Street, Dr. Roger Batzel, and Dr. Robert Goeckerman.

Significant help was received from Dr. Paul Concus in writing programs utilizing the IBM 704 and 709 computers, while Claudette Rugge was wholly responsible for the adaptation and running of MISFIT.

The continuous interest and support of Professor I. Perlman throughout all phases of this work are acknowledged.

APPENDIX I. AVERAGE SCATTERING POSITION OF NEUTRONS IN THE DETECTORS

The time of flight measured for a neutron depends on the distance it travels before producing a light pulse in the neutron detector. The distance is always at least the distance between the fission source and the face of the detector. However, there is an additional distance traveled by the neutron before it produces a proton recoil leading to the light pulse that is detected. In order to calculate the average distance traveled by neutrons it is now necessary to calculate the average distance from the face to the point at which a proton recoil is produced.

The plastic neutron detectors were 5.08 cm long. The probability ρ_x for neutron scattering as a function of distance into a detector is given by

$$\rho_x \approx \int_0^t e^{-x/\lambda}\frac{1}{\lambda}dx,$$

where λ = mean free path, x = distance from the face, and t = thickness of the detector.

The average distance of penetration x_0 of a neutron in a counter before it collides with a proton is given as

$$\bar{x}_0=\int_0^t \frac{xe^{-x/\lambda}}{\lambda}dx \Big/ \int_0^t \frac{e^{-x/\lambda}}{\lambda}dx.$$

For a 2-Mev neutron the value of $\bar{x}_0$ is approximately 2.22 cm, for a λ of 7.35 cm. The dispersion in the flight path can be found by solving for the second moment of the penetration probability, $\bar{x}^2$. This expression is

$$\bar{x}^2=\lambda^{-1}\int_0^t x^2e^{-x/\lambda}dx \Big/ \left(\lambda^{-1}\int_0^t e^{-x/\lambda}dx\right)$$

$$=\lambda^2[(t^2/\lambda^2+2t/\lambda+2)\exp(-t/\lambda)-2]/(e^{-t/\lambda}-1).$$

For a 2-Mev neutron, $\bar{x}^2=6.57$ cm^2. The variance is found by

$$\sigma^2=\bar{x}^2-\bar{x}_0^2=6.75-4.94=1.63 \text{ cm}^2.$$

The full width at half maximum of the dispersion is FWHM$=2.35\sigma=3$ cm. Thus an uncertainty of about 1.5% is introduced into the measurement of the time of flight because of a corresponding dispersion in the distance traveled by the neutrons.

APPENDIX II. RELATIONS INVOLVING $\varrho(V,\theta)$

Consider a number of fission events that have occurred in a certain run, the direction in space of the fission fragments being defined by the location of the fission counters (see Fig. 5). With each neutron emitted during the run we may associate a vector $\mathbf{V}$ specifying the magnitude and direction of the neutron velocity (in the laboratory system). The swarm of vector tips associated with a large number of neutrons defines a

certain distribution in the velocity space of the vectors $\mathbf{V}$. We denote the density of the swarm by $\rho(\mathbf{V})$, a function of the location $\mathbf{V}$ in velocity space. The normalization of $\rho(\mathbf{V})$ is assumed to be such that the integral of $\rho(\mathbf{V})$ over the whole of the velocity space—i.e., the integral over all neutron directions and velocities—is equal to the number of neutrons emitted per fission of Cf^{252},

$$\int \rho(\mathbf{V}) d^3V = \bar{\nu},$$

where $\bar{\nu}=3.82$ neutrons per fission.

The significance of $\rho(\mathbf{V})$ is then that $\rho(\mathbf{V})d^3V$ gives the number of neutrons per fission falling in the angular and velocity range defined by d^3V. (Another way to visualize $\rho(V,\theta)$ is to imagine that all fissions take place at a time zero. Then $\rho(V,\theta)$ is the spatial distribution of neutrons 1 nsec after fission.) Since there can be no dependence of ρ on the azimuthal angle β around the fission direction, the distribution $\rho(\mathbf{V})$ is a function only of the polar angle θ and the magnitude V. The relation between the function $\rho(V,\theta)$ and the experimental counting rates in the fission and neutron counters described in Sec. II is as follows:

The number of neutrons per fission with velocities between V and $V+\Delta V$ falling onto a neutron counter subtending a solid angle ω is $\rho(V,\theta)V^2\omega\Delta V$. (The factor $V^2\omega\Delta V$ is the volume of the velocity space in question in Fig. 5.) The relation between the velocity V and the flight time t is

$$t=D/V, \quad S=-(D/V^2)\Delta V,$$

where D is the flight distance of the neutron, so that the velocity interval ΔV is related by $\Delta V=-(V^2/D)S$ to the time interval S, as defined by the true width of a channel in the pulse-height analyzer.

The number of counts (per fission) registered in a channel is then

$$\epsilon_V \rho(V,\theta) V^2 \omega (V^2/D) S,$$

where ϵ_V is the counter efficiency for registering a neutron of velocity V. The number of counts N in a time interval S registered in a run in which R fissions occurred (as registered by the fission counters) is then

$$N=R\epsilon_V \rho(V,\theta)(V^4\omega/D)S,$$

from which it follows that the required function $\rho(V,\theta)$ is related to the observed quantities N, R, ϵ, ω, V, and S by

$$\rho(V,\theta)=ND/(R\epsilon V^4 \omega S).$$

APPENDIX III. ENERGY LOSS FOR FRAGMENTS IN Ni FOIL

The velocity correction due to the energy loss of fission fragments passing through nickel foil may be obtained from the range-energy relation for fission fragments given by Alexander and Gazdik,[24] ($R=CE^{\frac{3}{2}}$), where the range R is in mg/cm^2, energy E is in Mev, and the value of C for nickel may be estimated from the graph on p. 882 of reference 24: $C=0.271$ mg/cm^2 Mev$^{\frac{3}{2}}$.

Rearranging and differentiating, we have $\Delta E=\frac{2}{3}(R^{\frac{1}{3}}/C^{\frac{2}{3}})\Delta R$, Substituting for R, $\Delta E=(\frac{2}{3}E^{\frac{1}{3}}/C)\Delta R=(3E^{\frac{1}{3}}/2C)\Delta R$.

The velocity-energy relation for energy in Mev, velocity in units of 10^9 cm/sec, and mass in atomic weight units is $E=0.51835AV^2$. Differentiating gives $\Delta E=1.0367AV\Delta V$. Substituting for E and ΔE in the range-energy relation above, and solving for ΔV, we have $\Delta V=4.3\Delta R/V^{\frac{1}{3}}A^{\frac{2}{3}}$. The thickness ($\Delta R$) of the nickel target foil is 0.09 mg/cm^2; then $\Delta V=0.4/V^{\frac{1}{3}}A^{\frac{2}{3}}$. For average values of A and V we obtain an average correction $\Delta V\approx 0.015\times 10^9$ cm/sec.

APPENDIX IV. EVAPORATION FORMULAS

The data (Sec. IV) were analyzed by using the following three temperature-evaporation formulas:

$$\rho(V,\theta)=\rho_L+\rho_H,$$

where L and H refer to light and heavy fragments, respectively;

$$\rho_I=(2a^2/4\pi)\nu_I v_I B_I\{(\alpha_1/T_1^2)\exp(-av_I^2/T_1)+(\alpha_2/T_2^2)\exp(-av_I^2/T_2)+[1-(\alpha_1+\alpha_2)]/T_3^2\exp(-av_I^2/T_3)\};$$

$$B_I=1-A_2+\tfrac{3}{2}A_2\cos^2\psi_I,$$

where I refers to L or H.

Significance of some terms used in the above equation as defined below are illustrated in Fig. 5: V is velocity (lab) of the neutrons (cm/nsec), v is center-of-mass velocity of neutrons (cm/nsec), V_H is average velocity of heavy fragments, V_L is average velocity of light fragments, θ is laboratory-system angle between the neutron and the light fragment, ψ is center-of-mass angle between neutrons and fragments, $a=0.5228=E/v^2$, where E is in Mev and v is in cm/nsec, ν_L is number of neutrons per fission from light fragments, ν_H is number of neutrons per fission from heavy fragments, T_1, T_2, T_3 are temperatures pertaining to the neutron distributions, and α_1, α_2 are constants representing fractions of temperatures T_1 and T_2.

$$\alpha_1+\alpha_2+\alpha_3=1,$$
$$v_L^2=V^2+V_L^2-2VV_L\cos\theta,$$
$$v_H^2=V^2+V_H^2+2VV_H\cos\theta,$$
$$\cos\psi_L=(V\cos\theta-V_L)/v_L,$$
$$\cos\psi_H=(-V\cos\theta-V_H)/v_H.$$

Other symbols involved in the discussion of evaporation are as follows: $\eta=av^2$ is the neutron energy in the center-of-mass system (in Mev) and $\varphi(\eta,\psi)d\eta d\psi$ is the normalized probability of finding a neutron in the range η to $\eta+d\eta$ and ψ to $\psi+d\psi$.

[24] J. Alexander and F. Gazdik, Phys. Rev. **120**, 874 (1960).